FISEVIER

Contents lists available at ScienceDirect

# International Journal of Biological Macromolecules

journal homepage: www.elsevier.com/locate/ijbiomac





# Chemical structures and immunomodulatory activities of polysaccharides from *Polygonatum kingianum*

Nanyu Chen <sup>a,b,1</sup>, Yunzhang Ding <sup>b,c,1</sup>, Xuan Li <sup>b,d,1</sup>, Jiang Li <sup>b</sup>, Yongxian Cheng <sup>a</sup>, Yong Tian <sup>e,f</sup>, Yuncai Tian <sup>e,f</sup>, Mingyi Wu <sup>b,\*</sup>

- a Institute for Inheritance-Based Innovation of Chinese Medicine, School of Pharmacy, Shenzhen University Medical School, Shenzhen University, Shenzhen 518060,
- b State Key Laboratory of Phytochemistry and Plant Resources in West China, Kunming Institute of Botany, Chinese Academy of Sciences, Kunming 650201, China
- <sup>c</sup> College of Life Sciences and Technology, Tarim University, Alar, Xinjiang 843300, China
- d Key Laboratory for Forest Resources Conservation and Utilization, Southwest Mountains of China, Southwest Forestry University, Kunming 650224, China
- e Shanghai Zhenchen Cosmetics Co., Ltd., Shanghai 201415, China
- f Shanghai Zhizhenzhichen Technology Co., Ltd., Shanghai 201109, China

# ARTICLE INFO

# Keywords: Polygonatum kingianum Polysaccharides Fructan Physicochemical properties Immunomodulatory activity

#### ABSTRACT

The physicochemical properties of the polysaccharides in *Polygonatum kingianum*, a Chinese medicinal herb used for both medicine and food, have not been fully studied. This study isolated three polysaccharides (PKP-1, PKP-2, and PKP-3) from the dry rhizomes of *P. kingianum*, with an average molecular weight of approximately 3137 Da, 5341 Da and 3755 Da, respectively. Structural analysis showed that all the three polysaccharides are fructans with  $\beta$ -D-Fruf- $(2\rightarrow, \rightarrow 6)$ - $\beta$ -D-Fruf- $(2\rightarrow, \rightarrow 1)$ - $\beta$ -D-Fruf- $(2\rightarrow, \rightarrow 1, 6)$ - $\beta$ -D-Fruf- $(2\rightarrow and \rightarrow 6)$ - $\alpha$ -D-Glcp- $(1\rightarrow glycosidic bond type. Notably, PKP-2 contains both acetyl groups and trace amounts of mannose residues. Scanning electron microscopy indicated that each polysaccharide possesses unique surface morphology. Thermal analysis showed that the three polysaccharides have good thermal stability. Rheological studies further revealed that all the three polysaccharides are typical shear thinning fluids. In vitro experiments showed that PKP-1 and PKP-2 significantly promote the secretion of NO and cytokines (TNF-<math>\alpha$ , IL-6) in macrophages by activating the NF- $\alpha$ B signaling pathway, thereby demonstrating potential immunomodulatory activity. These findings lay a theoretical foundation for the potential application of *Polygonatum* polysaccharides in the food industry.

# 1. Introduction

Polygonatum (Liliaceae) was initially documented in the "Famous Physicians' Records "during the Eastern Han Dynasty in China and was listed as a top-grade herb. At present, the Traditional Chinese Medicine Polygonatum, also called as "Huangjing" in China, is defined as the dry rhizome of Polygonatum kingianum Coll. et Hemsl., Polygonatum sibiricum Red. or Polygonatum cyrtonema Hua in the Chinese Pharmacopoeia. It has the effects of nourishing qi and yin, strengthening the spleen, moistening the lungs, and tonifying the kidneys [1]. In addition, Polygonatum is used as both medicine and food, and is included in the Catalogue of Substances that are Both Food and Traditional Chinese Medicine [2]. There are also medicines and functional foods related to Polygonatum, such as Yiyuan Huangjing Syrup and P. sibiricum tea,

*P. sibiricum* cake and *P. sibiricum* wine [3]. All these indicate that the application of *Polygonatum* is very promising.

Polygonatum polysaccharide is considered as an important bioactive component [4]. Currently, many studies have focused on the pharmacological activities of *Polygonatum* polysaccharide, including antioxidant [5], immune regulatory [6], and prebiotic activities [7]. Our research group has previously done research on the prebiotic activity of *Polygonatum* polysaccharide [8], but less research has been done in the direction of its fluid food, in this work we surprisingly found that three polysaccharides from *P. kingianum* possess hydrocolloid feature, with a high degree of viscosity when dissolved in water. In order to improve the comprehensive utilization of *Polygonatum* polysaccharide as well as to develop its application in food industry, it is essential to study the structure, physicochemical properties and colloidal characteristics of

<sup>\*</sup> Corresponding author.

E-mail address: wumingyi@mail.kib.ac.cn (M. Wu).

 $<sup>^{1}</sup>$  These authors contributed equally to this work.

Polygonatum polysaccharide.

The rheological and thermal stability of polysaccharides are key factors for their ability to play important roles in the food industry. Rheological analysis was conducted to study the deformation and recovery ability of polysaccharide solution under external forces [9], which is crucial for understanding the transport and absorption mechanisms of polysaccharides in living organisms. The thermal analysis of polysaccharides can help us understand their behavior during the heating process [10], which is crucial for designing and optimizing the processing technology of polysaccharides, thus guiding their application and development.

In this study, we isolated three polysaccharides from *P. kingianum* and obtained information on their molecular weight, functional groups, monosaccharide composition, and glycosidic bond types through high-performance gel chromatography, UV–Visible analysis, FT-IR analysis, methylation analysis, 1D NMR analysis and 2D NMR analysis. Further rheological and thermal analysis studies were conducted to obtain information on the viscosity, elasticity, and thermal stability of polysaccharides. Subsequently, the immunomodulatory activities and underlying mechanisms of the three polysaccharides were assessed by using in vitro RAW264.7 macrophage assays.

# 2. Materials and methods

#### 2.1. Materials

The P. kingianum was purchased from Yunnan Lysheng Pharmaceutical Co., Ltd. (Yunnan, China) (Fig. S1). DEAE-52 cellulose was from GE Healthcare Life Science (Piscataway, NJ, USA). Standard dextrans were from National Institutes for Food and Drug Control (Beijing, China). The monosaccharide standards including D-fructose, D-glucose, D-glucuronic acid, D-galactose and D-galacturonic acid were from Sigma-Aldrich (Shanghai, China). D-mannose, L-Rhamnose, L-xylose and D-arabinose were from Alfa Aesar (Shanghai, China). L-Fucose was from Tokyo Chemical Industry (Tokyo, Japan). Trifluoroacetic acid (TFA), 1-phenyl-3-methyl-5-pyrazolone (PMP) and dimethyl sulfoxide (DMSO) were from Aladdin (Shanghai, China). Sodium borodeuteride (NaBD<sub>4</sub>) was from J&K Scientific Ltd. (Guangdong, China). Deuterium oxide (D2O) was from Cambridge Isotope Laboratories, Inc. (Cambridge, USA). Fetal bovine serum was sourced from Lonsera (Shanghai, China). The CCK-8 and NO detection kit were obtained from Suzhou Youvilandi Biotechnology Co., Ltd. (Suzhou, China). The DMEM medium was from Gibco (Grand Island, USA). The IL-6 and TNF-α assay kits were purchased from Invitrogen (California, USA). Lipopolysaccharide (LPS) was from Sigma (USA). The primary antibodies against phospho-NF-κB p65, NF-κB-p65, phosphor-IκBα, IκBα, and secondary antibodies were from the Cell Signaling Technology (Massachusetts, USA), and GAPDH from ABclonal Biotechnology (Wuhan, China).

#### 2.2. Extraction and purification of the polysaccharides

The detailed steps for polysaccharides extraction, separation, and purification are illustrated in Fig. S2. Briefly, the dried *P. kingianum* (300 g) was crushed and degreased with ethanol, dried in the air and extracted twice with deionized water (3 L) at 80 °C (2 × 2 h). The extract was combined and centrifuged (4000 rpm × 15 min). Afterwards the ethanol was added to the extraction solution until the final concentration is 40 % ( $\nu$ / $\nu$ ) and centrifuged (4000 rpm × 15 min) to obtain the precipitate PKP40. Then added ethanol to the supernatant until the final concentration is 60 % ( $\nu$ / $\nu$ ), and centrifuged (4000 rpm × 15 min) it to obtain the precipitate PKP60. Finally, ethanol was added to the supernatant until the final concentration is 80 % ( $\nu$ / $\nu$ ) followed by centrifugation (4000 rpm × 15 min) to obtain the precipitate PKP80.

For further purification, the PKP40 (4.867 g), PKP60 (2.932 g) and PKP80 (10.050 g) were dissolved by deionized water and passed through a DEAE-52 cellulose column (4.0 cm  $\times$  25.0 cm), and eluted with

deionized water (eluted with three times the column volume), respectively, and were named PKP40W, PKP60W, and PKP80W. Sephadex G-75 column was used to remove water-soluble macromolecules. The polysaccharide solutions were then dialyzed (MWCO 1000 Da) for 48 h and finally lyophilized to obtain the purified polysaccharides PKP-1, PKP-2 and PKP-3.

#### 2.3. Measurement of molecular weight

In accordance with the previously established method [11], the homogeneity, weight average molecular weight (Mw) and number average molecular weight (Mn) of polysaccharides were determined by high-performance gel permeation chromatography (HPGPC) using an Agilent technologies 1260 series (Agilent Co., USA) system equipped with a Shodex OHpak SB-804 HQ column (8  $\times$  300 mm). The molecular weight was calculated and calibrated using GPC software (Agilent Technologies, Inc., USA, version 3.4).

The standard curves were plotted using dextran standards with different known molecular weights (2700, 5250, 9750, 13,050, 36,800, 64,650, 135,350, and 300,600 Da). The mobile phase was 0.1 M NaCl, the flow rate was 0.5 mL/min, and the column temperature setting was maintained at 35  $^{\circ}\text{C}$ .

# 2.4. UV-visible and FT-IR spectra analysis

The UV-2600 (SHIMADZU, Japan) was used to record the absorbance of polysaccharides solution (1 mg/mL) with the range of 190 to  $800~\rm nm$ 

The FT-IR spectroscopy of purified polysaccharides in the range of  $400-4000~{\rm cm}^{-1}$  was determined using the KBr-pellets method on a FT-IR spectrometer (Tensor 27, Bruker, Germany).

# 2.5. Monosaccharide composition analysis

The monosaccharide composition was determined by PMP pre column derivatization method. In brief, the purified polysaccharides were dissolved in a COD tube in 2 M TFA and react at 110 °C for 4 h. Then methanol was added three times to spin dry it. Added 0.6 M NaOH and 0.5 M PMP methanol solutions to the samples, and incubated at 70 °C for 1 h. Cooled to room temperature and added 0.6 M HCl to stop the reaction. Finally, extracted three times with CHCl3. The processing process of monosaccharide standards was the same as that of samples.

The samples were analyzed on Agilent technologies 1260 series system (Agilent Co., USA) with a XSelect HSS T3 column (4.6  $\times$  250 mm, 5  $\mu m$ ). The mobile phase was a mixture of 0.1 M phosphate buffer and CH $_3$ CN (82:18), the flow rate was 1 mL/min, the column temperature setting was maintained at 25  $^{\circ}$ C, and entire analysis process was monitored by a diode array detector (DAD) at 250 nm.

Considering the complex composition of polysaccharides, an additional assay was conducted to ensure more precise results. In sum, the purified polysaccharides were dissolved in a COD tube in 0.5 M TFA and react at 100  $^{\circ}\text{C}$  for 2 h. Then added methanol three times to spin dry it. Finally dissolved, centrifuged (13,000 rpm  $\times$  15 min), filtered and waited for injection. The processing process of monosaccharide standards was the same as that of samples.

The samples were analyzed on Agilent technologies 1260 series system (Agilent Co., USA) with a Cosmosil Sugar-D column (4.6  $\times$  250 mm, 5  $\mu m$ ). The mobile phase was a mixture of ultrapure water and CH<sub>3</sub>CN (15:85), the flow rate was 0.2 mL/min, the column temperature setting was maintained at 35  $^{\circ}$ C, and entire analysis process was monitored by a refractive index detector (RID).

# 2.6. Methylation and GC-MS analysis

2.6.1. Preparation of the partially methylated alditol acetates (PMAAs)

The methylation of polysaccharide was generally carried out using

the Needs method with minor modifications [12]. Briefly, dissolved the polysaccharides in anhydrous DMSO and added them to a prepared DMSO solution of NaOH (50 mg/mL). Stirred with magnetic force to dissolve. Added CH<sub>3</sub>I to react for 3 h under ice bath and dark conditions, extracted three times with CHCl<sub>3</sub>, and then extracted three times with deionized water. Took the organic phase and spin dried it. Added 0.5 M TFA and hydrolyzed at 70 °C for 3 h, then added methanol and spin dried. Added NaOH solution to achieve a pH value of 10, reacted at 50 °C for 2 h with NaBD<sub>4</sub>, and spin dried with methanol. Added acetic anhydride and pyridine to react at 100 °C for 1 h and extracted with CH<sub>2</sub>Cl<sub>2</sub>, and then extracted three times with deionized water to obtain PMAAs in the organic phase.

# 2.6.2. GC-MS analysis

The PMAAs were analyzed on HP6890GC/5973 MS system (Agilent Co., USA) equipped with a HP-5MS quartz capillary column (30 m  $\times$  0.25 mm, 0.25 µm film thickness). GC conditions were set as follows: The initial temperature of the column was 80 °C, maintained for 1 min, and after a programmed temperature rose of 5 °C/min to 250 °C, maintained for 40 min. The column flow rate was 1.5 mL/min. The injection port temperature was 250 °C. The pre-column pressure was 100 kPa. The split ratio was 10:1. The carrier gas was high-purity helium. The injection volume was 1 µL. MS conditions were set as follows: The ionization method was EI. The electronic energy was 70 eV. The transmission line temperature was 290 °C. The ion source temperature was 230 °C. The quadrupole temperature was 150 °C. The mass range was m/  $^{\circ}$  50.600

GC-MS data analysis should be compared to the standard chromatogram of the Complex Carbohydrate Research Center (CCRC) database (https://www.ccrc.uga.edu).

# 2.7. Nuclear magnetic resonance (NMR) spectroscopy analysis

The purified polysaccharides were dissolved in  $D_2O$  and lyophilized three times to complete deuterium exchange.  $^1H$ ,  $^{13}C$ ,  $^1H$ — $^1H$  correlated spectroscopy ( $^1H$ — $^1H$  COSY),  $^1H$ — $^{13}C$  heteronuclear single-quantum coherence (HSQC), heteronuclear multiple bond coherence (HMBC),  $^1H$ — $^{13}C$  HSQC-TOCSY and distortionless enhancement by polarization transfer-135 (DEPT-135) NMR spectra were recorded by a Bruker Avance 800 MHz spectrometer (Bruker, Germany) equipped with  $^1H$ — $^{13}C$  dual probes in FT mode.

Sodium 3- (trimethylsilyl) propionate (TMSP,  $\delta_H$  and  $\delta_C=0.00$ ) was used as internal standard for NMR analysis.

#### 2.8. Scanning electron microscope analysis

After the polysaccharide sample had been freeze-dried, a small amount of the sample was weighed and immersed in a conductive adhesive. The powder that had not adhered to the conductive adhesive was blown off, then the sample was sprayed with gold and tested under an electron microscope (SEM; Hitachi, S4800, Japan). The samples were observed at 500 or 1000 magnification.

# 2.9. Thermal characterization

The thermal characteristics of the sample were determined using thermogravimetric analysis (TG) and differential scanning calorimetry (DSC) on a thermogravimetric analyzer (SDT Q600, TA instruments, USA). Weighed a small amount of sample (about 5 mg) and placed it in a crucible. Opened the instrument and placed the crucible in the instrument. Heated it from 25 °C to 800 °C at a heating rate of 10 °C/min under a nitrogen atmosphere, with a flow rate of 100 mL/min.

# 2.10. Rheological properties

Measured the rheological properties of polysaccharides using a

rheometer (Kinexus ultra, Netzsch, Germany) equipped with parallel plate geometry (PU20 SR5612SS, 20 mm diameter, 0.15 mm gap).

# 2.10.1. Steady-state shear test

Plotted the shear rate viscosity relationship curve for a 4 % (w/v) aqueous solution at a shear rate range of 0.01 to 1000 s<sup>-1</sup> at 25 °C.

#### 2.10.2. Dynamic rheological test

Measured the storage modulus (G') and loss modulus (G") of a 4 % (w/v) aqueous solution in the angular frequency range of 0.01 to 100 rad/s at 5 % strain at 25  $^{\circ}$ C.

# 2.11. Immunomodulatory activity assay

#### 2.11.1. Cell culture

RAW264.7 cells were cultured in DMEM medium containing 10 % ( $\nu/\nu$ ) fetal bovine serum (FBS) and 1 % penicillin/streptomycin, under cell culture conditions of 5 % CO<sub>2</sub> and 37 °C.

# 2.11.2. Cell viability

RAW264.7 cells were plated at a density of  $1\times10^4$  cells/well in a 96-well plate and incubated in a 5 % CO $_2$ , 37 °C cell culture incubator for 24 h. The cells were then treated with PKP-1, PKP-2, and PKP-3 at concentrations of 50  $\mu g/mL$ , 150  $\mu g/mL$ , and 450  $\mu g/mL$ , along with 1  $\mu g/mL$  LPS, for 24 h. Subsequently, 10  $\mu L$  of CCK-8 solution was added to each well and the plate was incubated at 37 °C in darkness for 2 h. Following this incubation, the optical density (OD) at 450 nm was measured using a microplate reader. Three replicate wells were used for each sample.

# 2.11.3. The secretion of inflammatory cytokines NO, IL-6, and TNF- $\alpha$

RAW264.7 cells were seeded at a density of  $1\times10^5$  cells/well in a 24-well plate and incubated in a 5 % CO $_2$ , 37 °C environment for 24 h. Subsequently, cells were treated with different concentrations of PKP-1, PKP-2, and PKP-3 (50  $\mu g/mL$ , 150  $\mu g/mL$ , and 450  $\mu g/mL$  respectively) along with 1  $\mu g/mL$  of LPS for 24 h. Nitric oxide (NO) levels were assessed using the Griess method, while IL-6 and TNF- $\alpha$  secretion in the supernatant were quantified using ELISA.

# 2.11.4. Western blot analysis

RAW264.7 cells were seeded in 6-well plates at a density of  $1\times10^6$  cells/well and treated with PKP-1, PKP-2, and PKP-3 at concentrations of 50 µg/mL, 150 µg/mL, and 450 µg/mL, along with 1 µg/mL LPS, for 24 h. Cellular proteins were extracted using RIPA lysis buffer supplemented with 1 % protease inhibitors and 1 % phosphatase inhibitors. Following the determination of protein concentration, the proteins were separated using 10 % SDS-PAGE and subsequently transferred to a PVDF membrane. The membrane was blocked with 5 % bovine serum albumin for 2 h at room temperature before being incubated overnight at 4 °C with primary antibodies (p-P65, P65, p-IkBa, IkBa, and GAPDH). After washing with TBST, the membrane was incubated with secondary antibodies for 2 h at room temperature. Finally, the blots were imaged using an Alliance MINI HD 9 imaging system (UVItec Limited, Cambridge, UK).

# 2.11.5. Data processing and analysis

Statistical analysis and graphing of data were conducted using GraphPad Prism 8.0. The data are presented as mean  $\pm$  standard deviation (SD), and the experimental results were assessed for significance using one-way ANOVA. P < 0.05 is considered statistically significant.

# 3. Results and discussion

# 3.1. Extraction and purification

The crude polysaccharides PKP40, PKP60 and PKP80 were extracted

**Table 1** Purification yields, molecular weight and molecular weight distribution of PKP-1, PKP-2 and PKP-3.

Samples	Dry weight (mg)	Purification yield (%)	Weight-average molecular weight (Mw, Da)	Number-average molecular weight (Mn, Da)	Polydispersity index (Mw/ Mn)
PKP-1	779.08	16.0	3137	2375	1.32
PKP-2	314.47	10.7	5341	3014	1.77
PKP-3	8604.8	85.6	3755	2684	1.40

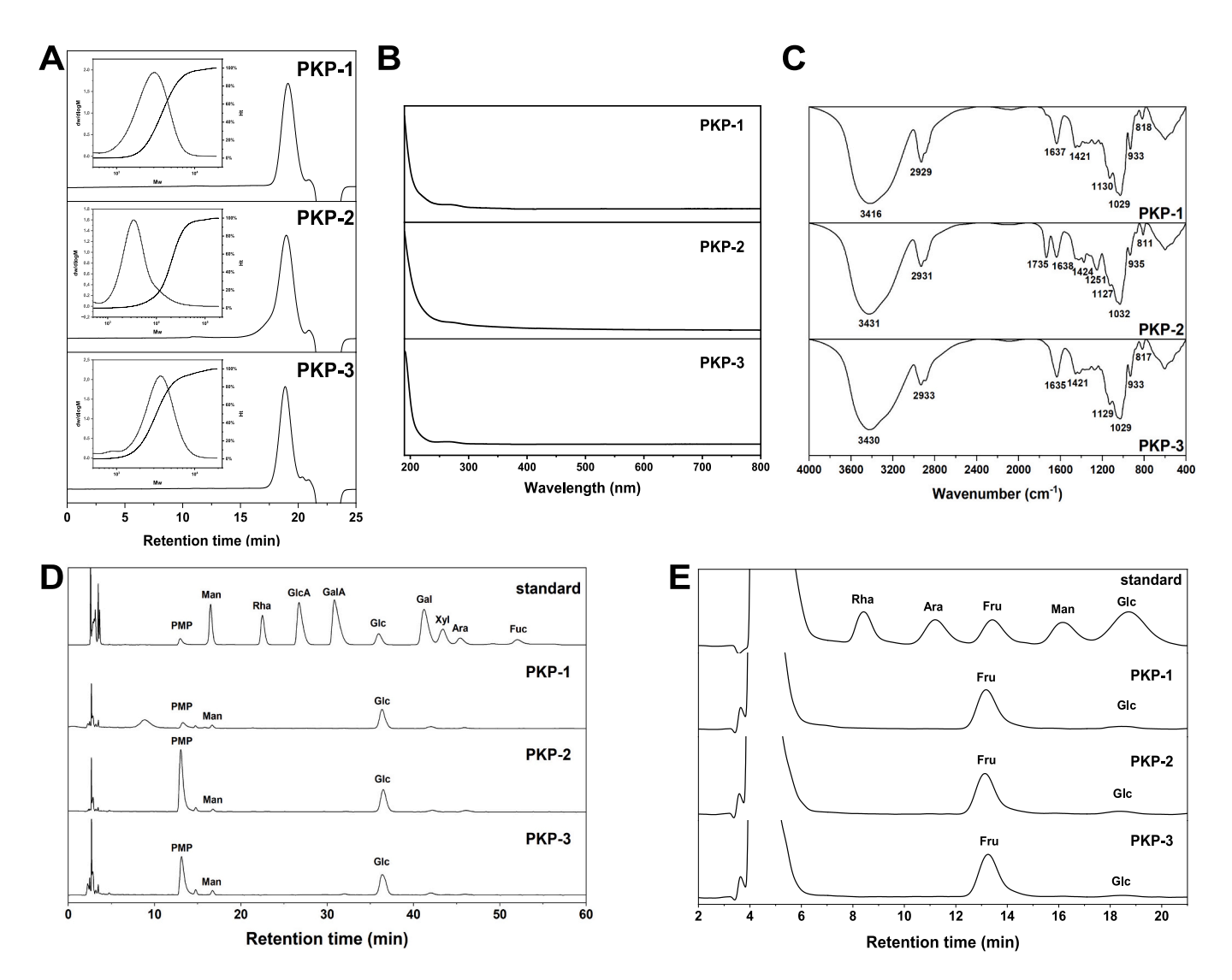


Fig. 1. Molecular weights, monosaccharide composition, UV-visible spectra and FT-IR spectra of PKP-1, PKP-2 and PKP-3. (A) HPGPC diagrams and molecular weight distributions of polysaccharides; (B) UV-visible spectra; (C) FT-IR spectra; (D) HPLC-DAD diagrams of standard monosaccharides and sample polysaccharides; (E) HPLC-RID diagrams of standard monosaccharides and sample polysaccharides.

from *P. kingianum* using hot water extraction and ethanol fractionation precipitation methods (Fig. S2). The extraction yields of three crude polysaccharides were 2.2 %, 1.4 % and 15.6 %, respectively (Table S1). PKP40, PKP60 and PKP80 were further purified using DEAE-52 and Sephadex G-75 columns to obtain three purified polysaccharides, PKP-1, PKP-2 and PKP-3. Purification yields of refined polysaccharides were 16.0 %, 10 % and 85.7 %, respectively (Table 1). The HPGPC profiles of the three purified polysaccharides showed single peaks and symmetry, indicating that all the three polysaccharides are relatively homogeneous polymers.

# 3.2. Molecular weight and molecular weight distribution

The weight-average molecular weight (Mw), number-average molecular weight (Mn) and polydispersity index (Mw/Mn) of purified polysaccharides were calculated using GPC software (Table 1). The distribution curve for the molecular weight was illustrated in Fig. 1A. The polydispersity index (PDI, Mw/Mn) serves as an indicator of the molecular weight distribution of polysaccharides, a lower value suggests a more concentrated distribution. The HPGPC diagrams, along with the PDI and molecular weight distribution curves for the three purified polysaccharides, indicate their high purity and homogeneity.

**Table 2** GC–MS signal attribution of methylation products of PKP-1, PKP-2 and PKP-3.

Samples	Type of linkages	Retention time (min)	Molar ratios	Mass fragments (m/z)
PKP-1	Terminal Fruf	19.938	9.04	87, 101, 129, 145, 162, 205
	2,6-Linked Fruf	22.637	1.47	87, 129, 146, 162, 189, 206, 233
	1,2-Linked Fruf	22.793	12.53	87, 101, 129, 145, 161, 190, 234
	1,6-Linked Glcp	23.466	1.00	87, 102, 118, 129, 162, 189, 233
	1,2,6-Linked Fruf	25.302	3.02	87, 99, 129, 190, 234
PKP-2	Terminal Fruf	19.952	6.56	87, 101, 129, 145, 162, 205
	2,6-Linked Fruf	22.647	0.82	87, 129, 146, 162, 189, 206, 233
	1,2-Linked Fruf	22.784	6.01	87, 101, 129, 145, 161, 190, 234
	1,4-Linked Glcp	22.984	0.30	87, 99, 118, 129, 162, 173, 233
	1,6-Linked Glcp	23.488	1.00	87, 102, 118, 129, 162, 189, 233
	1,2,6-Linked Fruf	25.296	1.10	87, 99, 129, 190, 234
PKP-3	Terminal Fruf	19.900	4.93	87, 101, 129, 145, 162, 205
	2,6-Linked Fruf	22.624	2.42	87, 129, 146, 162, 189, 206, 233
	1,2-Linked Fruf	22.744	11.49	87, 101, 129, 145, 161, 190, 234
	1,6-Linked Glcp	23.448	1.00	87, 102, 118, 129, 162, 189, 233
	1,2,6-Linked Fruf	25.290	4.07	87, 99, 129, 190, 234

# 3.3. UV- visible and FT-IR spectra analysis

The UV-visible spectra of PKP-1, PKP-2 and PKP-3 are depicted in Fig. 1B, no obvious absorptions at 260 nm and 280 nm were observed, indicating that no nucleic acids or proteins were presented in the polysaccharide samples.

The FT-IR spectra was used to analyze the main functional groups and configurations of polysaccharides. As shown in the Fig. 1C, taking the PKP-2 as an example, the broad and intense peak at 3431 cm $^{-1}$  was ascribed to the O—H stretching vibration. The peak at 2931 cm $^{-1}$  was attributed to the stretching vibration of C—H in the sugar ring [13]. The characteristic absorption peak at 1638 cm $^{-1}$  was probably due to the associated water [14]. The peak at 1424 cm $^{-1}$  was attributed to the bending vibration of C—H. The prominent peaks at 1032 cm $^{-1}$  and 1127 cm $^{-1}$  were ascribed a pyranose form of polysaccharides [15]. The signal at 935 cm $^{-1}$  and 811 cm $^{-1}$  were assigned to the  $\beta$ -type glycosidic linkages [16,17]. In addition, PKP-2 showed absorption peaks at 1735 cm $^{-1}$  and 1251 cm $^{-1}$  attributed to the C—O stretching vibration and the C—O stretching vibration in the O-acetyl group, respectively [18,19], indicating the presence of acetyl groups, where PKP-2 was different from other polysaccharides.

# 3.4. Monosaccharide composition analysis

The monosaccharide compositions of PKP-1, PKP-2 and PKP-3 were determined by PMP pre-column derivatization method (Fig. 1D), and by direct analysis after acid hydrolysis (Fig. 1E). Fig. 1D displayed the HPLC profiles of nine mixed standard monosaccharides: mannose, rhamnose, gluconic acid, galacturonic acid, glucose, galactose, xylose, arabinose, and fucose. In addition, all of polysaccharides contain major glucose and a small amount of mannose by contrasting the retention time of standard monosaccharides. The HPLC profiles for the three polysaccharides revealed a high peak for fructose and a low peak for

glucose (Fig. 1E), and mannose was not identified on the profile due to its low content. The peak area ratios of fructose to glucose in PKP-1, PKP-2, and PKP-3 were 10.91: 1.00, 11.29: 1.00, and 19.08: 1.00, respectively. The results suggested that these polysaccharides may be classified as fructans.

#### 3.5. Methylation and GC-MS analysis

Methylation analysis is pivotal in determining the type of poly-saccharide linkage. The total ion chromatogram (TIC) profiles of partially methylated alditol acetates (PMAAs) of purified poly-saccharides were illustrated in Fig. S3. Compared the GC-EIMS database of PMAAs (Complex Carbohydrate Research Center, University of Georgia) and the acquired mass spectra, the connection types, molar ratios, and main fragments were shown in Table 2.The ion chromatographic peaks of all polysaccharides were identified as Terminal Fruf, 2,6-Linked Fruf, 1,2-Linked Fruf, 1,6-Linked Glcp and 1,2,6-Linked Fruf (Fig. S3). Furthermore, the peak of PKP-2 in the ion chromatography was identified as having one additional peak compared to the others, which is identified as 1,4-Linked Glcp.

Because it is difficult to obtain a standard for each monosaccharide derivative, it is not possible to accurately determine the ratio of each linkage [20]. However, the result indicated that the polysaccharides have the most 2,1-linked Fruf fragments, which may form the backbone of the polysaccharides. These structures could be confirmed by the following NMR analysis.

#### 3.6. NMR spectra analysis

NMR spectral analysis is one of the most useful techniques for identifying polysaccharide structures. It is primarily utilized in the characterization of polysaccharides, encompassing heteromeric configurations ( $\alpha$ - or  $\beta$ -), as well as the types and sequences of glycosidic bonds [21]. Thus, we further used NMR technology to analyze these polysaccharides. Their 1D and 2D NMR spectra were shown in Figs. 2–3, and Figs. S4-S5. Their  $^1H$  and  $^{13}C$  NMR chemical shifts were presented in Table 3.

# 3.6.1. NMR spectra analysis of PKP-1 and PKP-3

In the 1D NMR spectra, one anomeric proton signal ( $\delta_{\rm H}$  5.42) and four anomeric carbon signals (approximately  $\delta_{\rm C}$  106.0–107.0) indicated that they might be a typical fructan [22,23] (Fig. 2A and B), and the absence of a characteristic signal at the 106.0–107.0 ppm anomeric carbon region on the DEPT-135 spectra (Fig. S4E—F), indicating that this region is a quaternary carbon signal [24,25]. In addition, these carbon signals do not have cross peaks in the HSQC spectrum and also conform to the characteristics of fructose residues.

Based on literature reports [26] and combined with methylation analysis results (Table 2), it was inferred that these four carbon signals ( $\delta_{\rm C}$  106.72, 106.88, 106.57 and 106.10) should belong to the C-2 signal of  $\beta$ -D-Fruf-(2 $\rightarrow$ , 6)- $\beta$ -D-Fruf-(2 $\rightarrow$ , designated as A, B, C and D, respectively. The remaining anomeric carbon signal ( $\delta_{\rm C}$  95.04) should be attributed to the other sugar residue and marked as E.

For residue E, the weak anomeric signals at  $\delta_H$  5.42 and  $\delta_C$  95.04 corresponded to a sugar residue with relatively low content, demonstrating that residue E was  $\alpha$ -configuration. Other the  $^1H$  and the corresponding  $^{13}C$  signals were assigned by COSY and HSQC spectra, respectively. According to the previous reports [8] and the results of methylation analysis, it could be inferred that residue E was  $\rightarrow$ 6)- $\alpha$ -D-

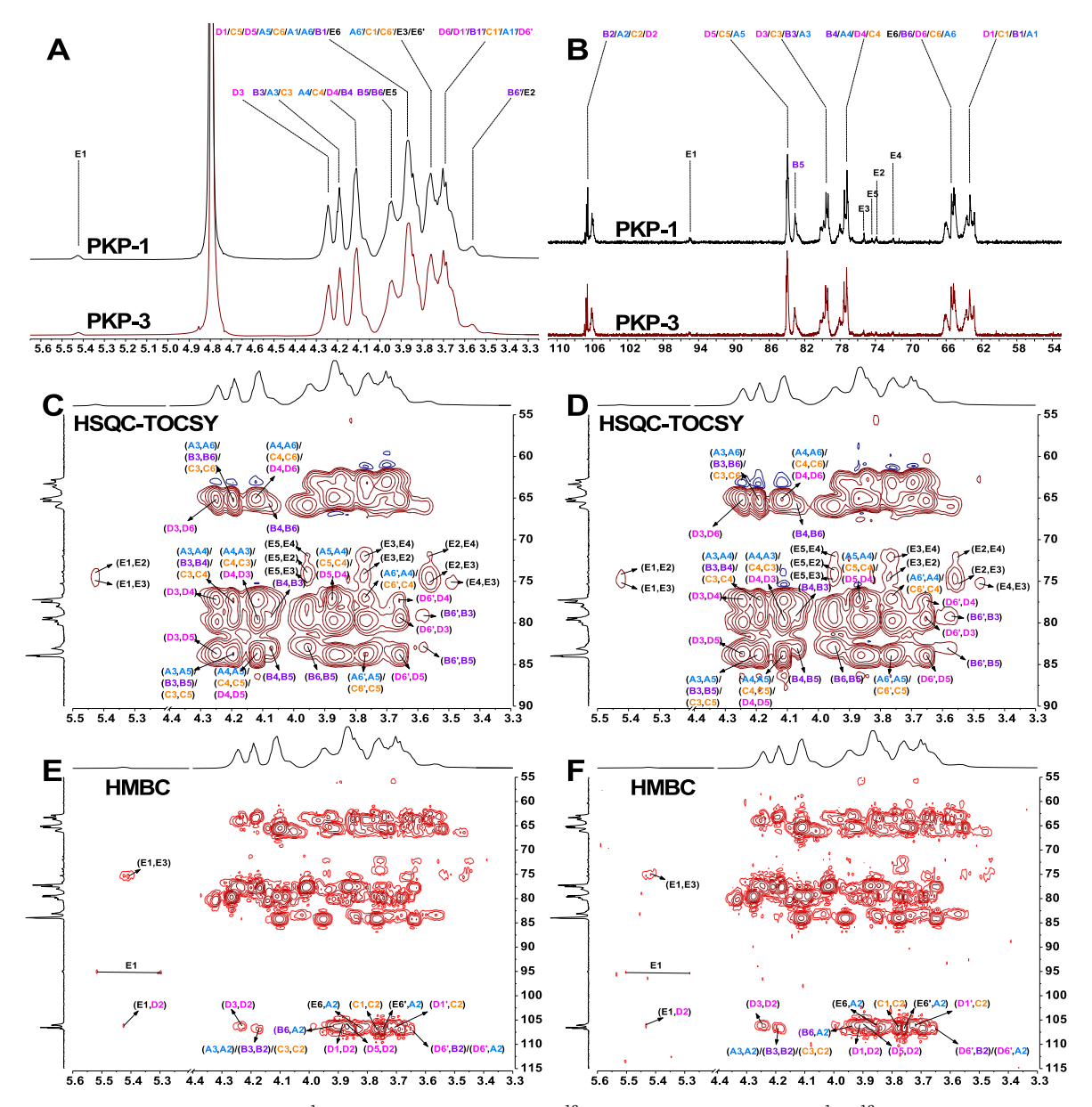


Fig. 2. The NMR spectra of PKP-1 and PKP-3. (A)  $^{1}$ H NMR of PKP-1 and PKP-3; (B)  $^{13}$ C NMR of PKP-1 and PKP-3; (C)  $^{1}$ H— $^{13}$ C HSQC-TOCSY of PKP-1; (D)  $^{1}$ H— $^{13}$ C HMBC of PKP-1; (F)  $^{1}$ H— $^{13}$ C HMBC of PKP-3. The A (grayish blue), B (purple), C (orange), D (magenta) and E (black) represent β-D-Fruf-(2 $\rightarrow$ ,  $\rightarrow$ 6)-β-D-Fruf-(2 $\rightarrow$ ,  $\rightarrow$ 1)-β-D-Fruf-(2 $\rightarrow$ ,  $\rightarrow$ 1,6)-β-D-Fruf-(2 $\rightarrow$  and  $\rightarrow$ 6)-α-D-Glcp-(1 $\rightarrow$ , respectively. (For interpretation of the references to colour in this figure legend, the reader is referred to the web version of this article.)

Glcp- $(1\rightarrow$ .

In <sup>1</sup>H—<sup>13</sup>C HMBC spectra (Fig. 2E and F), cross peaks were found between H-6/6′ of residue E (3.83/3.76 ppm) and C-2 of residue A (106.72 ppm); H-1 of residue E (5.42 ppm) and C-2 of residue D (106.10 ppm); H-1 of residue C (3.77 ppm) and C-2 of its own (106.57 ppm); H-1′ of residue D (3.72 ppm) and C-2 of residue C (106.57 ppm). These signals formed the main chains of PKP-1 and PKP-3. The cross peaks between H-6′ of residue D (3.65 ppm) and C-2 of residue A (106.72 ppm), indicated that residue A is linked to residue D at the O-6 position. The cross peaks between H-6′ of residue D (3.65 ppm) and C-2 of residue D at the O-6 position. The cross peaks between H-6 of residue B is linked to residue D at the O-6 position. The cross peaks between H-6 of residue A (106.72 ppm), indicated that residue A is linked to residue B at the O-6 position. The proposed chemical structures of PKP-1 and PKP-3 were shown in Fig. 4A.

# 3.6.2. NMR spectra analysis of PKP-2

The 1D (<sup>1</sup>H and <sup>13</sup>C) NMR, HSQC, and DEPT-135° spectra of PKP-2 were shown in Fig. 3.In the 1D NMR spectra of PKP-2, it could be seen that <sup>1</sup>H and <sup>13</sup>C NMR data are familiar with those of PKP-1 (Fig. 3A and B). According to COSY and HSQC spectra, the chemical shifts of <sup>1</sup>H and <sup>13</sup>C of the residues A, B, C, D and E are similar to those of PKP-1, indicating that PKP-2 is still a fructan.

The <sup>1</sup>H NMR spectra of PKP-2 at 2.12–2.19 ppm and the <sup>13</sup>C NMR spectra of PKP-2 at 22.91–23.41 ppm and 175.58–176.81 ppm infer that PKP-2 contains acetyl groups and that the acetyl groups are substituted at different positions [28], where PKP-2 differs from PKP-1. In HSQC spectrum, the anomeric region signals 4.77/103.27 ppm, 4.95/102.12 ppm and 4.83/102.66 ppm were attributed to the mannose residue, additionally the cross-peak signals 4.53/4.28/65.89 ppm also belonged to the H6/C6 position of the mannose residue [29,30], marked as G, H, I and *J.* 4.50/105.64 ppm was marked as F (Fig. 3C).

Other the <sup>1</sup>H and the corresponding <sup>13</sup>C signals of the residues F, G,

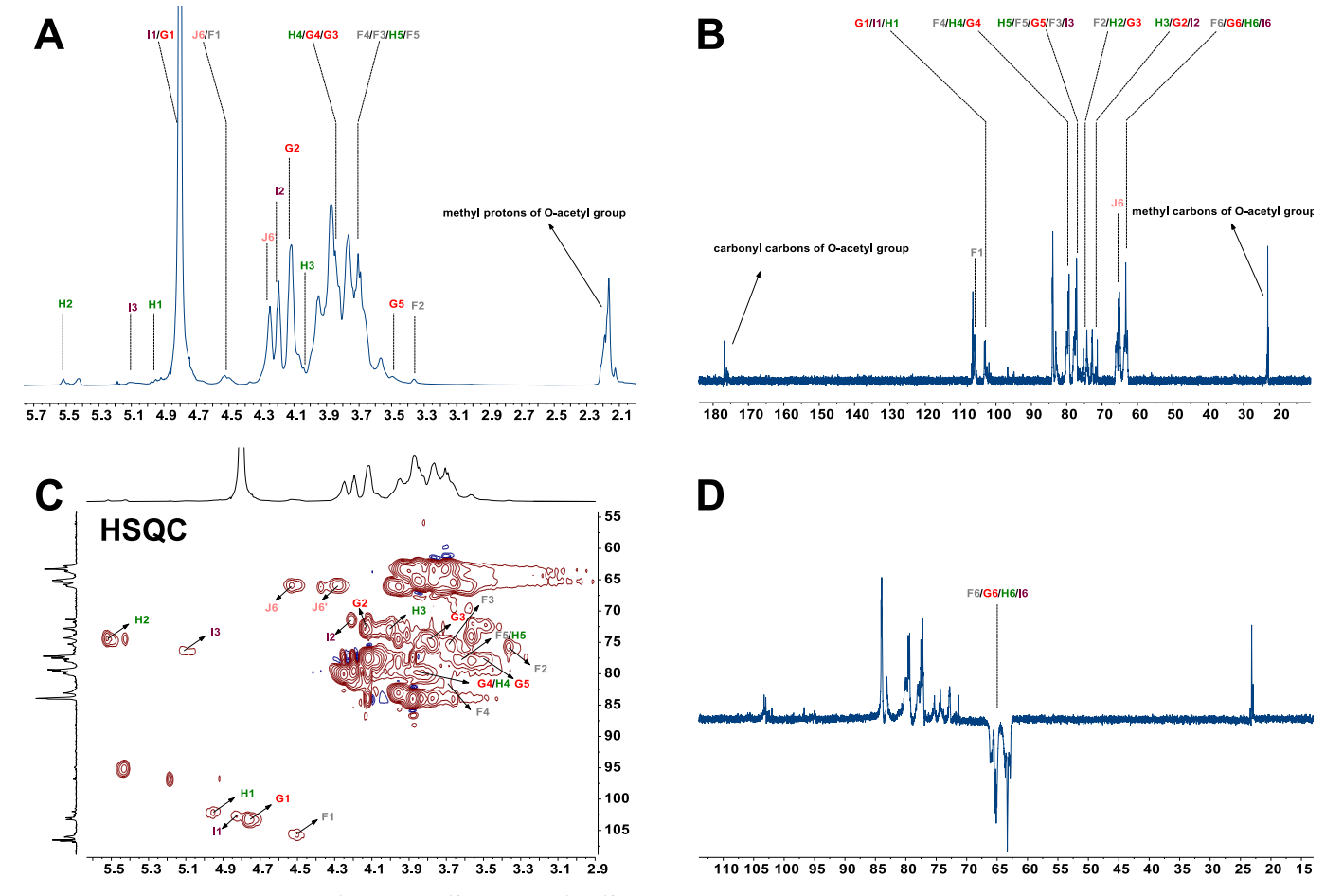


Fig. 3. The NMR spectra of PKP-2. (A)  $^{1}$ H NMR; (B)  $^{13}$ C NMR; (C)  $^{1}$ H— $^{13}$ C HSQC; (D) DEPT 135°. The F (grey), G (red), H (green), I (dark purple) and J (pink) represent  $\rightarrow$ 4)- $\beta$ -D-Glcp-(1 $\rightarrow$ ,  $\rightarrow$ 4)- $\beta$ -D-Manp-(1 $\rightarrow$ ,  $\rightarrow$ 4)-2-O-acetyl- $\beta$ -D-Manp-(1 $\rightarrow$ ,  $\rightarrow$ 4)-3-O-acetyl- $\beta$ -D-Manp-(1 $\rightarrow$ , respectively. (For interpretation of the references to colour in this figure legend, the reader is referred to the web version of this article.)

H, I and J were assigned by COSY and HSQC spectra. Due to their relatively low content, the signals could not be completely found. According to the previous reports [31] and the results of monosaccharide composition analysis and methylation analysis, they could be inferred as  $\rightarrow$ 4)-β-D-Glcp-(1 $\rightarrow$ ,  $\rightarrow$ 4)-β-D-Manp-(1 $\rightarrow$ ,  $\rightarrow$ 4)-2-O-acetyl-β-D-Manp-(1 $\rightarrow$ , and  $\rightarrow$ 4)-6-O-acetyl-β-D-Manp-(1 $\rightarrow$ . In HMBC spectrum, due to the low content of mannose (Fig. 1), no connection signal with the sugar chain was found, several speculated structures were shown in Figs. 5B. According to the biosynthetic pathway of fructan [32], the three *P. kingianum* fructans may belong to Graminans series. Therefore, it was speculated that mannose residues are connected to side chains.

These *P. kingianum* polysaccharides all belong to fructans, and their differences displayed that PKP-2 contains acetyl groups. Based on the integral ratio between the anomeric protons in the  $\alpha$ -pyranose residues and the non-overlapping proton signals of H-3 or H-4 of the  $\beta$ -fructo-furanose residues, the glucose content of PKP-1 is relatively high (Fig. S6), which was consistent with the results of monosaccharide composition analysis (Fig. 1D). Our research group isolated an agavin fructan from *P. cyrtonema* Hua previously [8]. In this work, we found a new type of fructan PKP-2 (with acetyl substitution) from *P. kingianum*. Thus the structural differences of fructans may be depended on their species.

# 3.7. SEM analysis

The surface topography and structure of a polysaccharide may be influenced by different methods of extraction, purification and

preparation [33]. SEM of the three polysaccharides were shown in Fig. S7. The results revealed that PKP-1 has a flat and smooth surface as well as a porous structure and has distinct pores with a diameter of  $8-10\,\mu$ m. For the samples containing acetyl groups, a significant difference between them can be observed. Fig. S7B illustrates that PKP-2 has a rough surface and PKP-2 exhibits irregular particles with tile-like granules, which is consistent with polysaccharides obtained from *Inonotus obliquus* [34]. For Fig. S7C, the absence of acetyl groups and low glucose content in sample PKP-3, the sample appears as unevenly sized fragments with no uniform void structure, suggesting that the glucose content plays a role in the integrity and smoothness of the polysaccharide.

#### 3.8. Thermal characterization

TG plots (Fig. 5) showed the thermal stability and decomposition behavior of three different polysaccharides. The TG curve of PKP-1 started to deviate from 100 % mass around 200 °C, indicating that some form of thermal event, either dehydration or volatilization of low molecular weight constituents, started to occur at this temperature [35]. The mass loss continued to stabilize, indicating that the rate of decomposition remains constant as the temperature increases. At roughly 600 °C the curve plateaued and approached a more stable mass percentage, implying that most of the combustible polysaccharide had been depleted, leaving behind a more thermally stable substance, potentially coke. PKP-3 had the lowest mass loss after 300 °C, indicating the highest onset temperature thermal stability of the three samples. This also implied that PKP-2 and PKP-3 contain more thermally stable

**Table 3**  $^{1}$ H and  $^{13}$ C NMR chemical shifts of polysaccharides PKP-1, PKP-2 and PKP-3 ( $\delta$  in ppm, J in Hz, in D<sub>2</sub>O).

Samples	Monosaccharide units	Chemical shifts (ppm)						
		H1/H1′/C1	H2/C2	H3/C3	H4/C4	H5/C5	H6/H6′/C6	
PKP-1	A β-D-Fruf-(2→	3.84/3.65	/	4.19	4.12	3.86	3.84/3.77	
		62.84	106.72	79.41	77.55	83.94	65.05	
	$\mathbf{B} \rightarrow 6$ )- $\beta$ -D-Fruf-(2 $\rightarrow$	3.83/3.69	/	4.20	4.07	3.95	3.95/3.58	
		63.04	106.88	79.47	77.81	83.13	66.03	
	$C \rightarrow 1$ )- $\beta$ -D-Fruf-(2 $\rightarrow$	3.77/3.69	/	4.19	4.11	3.87	3.84/3.77	
		63.35	106.57	79.64	77.26	83.98	65.17	
	$\mathbf{D} \rightarrow 1,6$ )- $\beta$ -D-Fruf-(2 $\rightarrow$	3.90/3.72	/	4.24	4.10	3.87	3.73/3.65	
	***	63.67	106.10	79.90	77.40	84.08	65.43	
	$E \rightarrow 6$ )- $\alpha$ -D-Glcp- $(1 \rightarrow$	5.42	3.57	3.77	3.48	3.95	3.83/3.76	
		95.04	73.89	75.32	72.02	74.45	66.17	
PKP-2	A β-D-Fruf-(2→	3.84/3.65	/	4.19	4.12	3.86	3.84/3.77	
		62.84	106.72	79.41	77.55	83.94	65.05	
	<b>B</b> $\rightarrow$ 6)- $\beta$ -D-Fruf-(2 $\rightarrow$	3.83/3.69	/	4.20	4.07	3.95	3.95/3.58	
	, k <del>d</del> (-	63.04	106.88	79.47	77.81	83.13	66.03	
	$C \rightarrow 1$ )- $\beta$ -D-Fruf- $(2 \rightarrow$	3.77/3.69	/	4.19	4.11	3.87	3.84/3.77	
	5 · 1)   2 11d) (2 ·	63.35	106.57	79.64	77.26	83.98	65.17	
	$\mathbf{D} \rightarrow 1,6$ )- $\beta$ -D-Fruf-(2 $\rightarrow$	3.90/3.72	/	4.24	4.10	3.87	3.73/3.65	
	,-, <sub>F</sub> <del>-</del> , (-	63.67	106.10	79.90	77.40	84.08	65.43	
	$E \rightarrow 6$ )- $\alpha$ -D-Glcp- $(1 \rightarrow$	5.42	3.57	3.77	3.48	3.95	3.83/3.76	
	2 · 0) w 2 didp (1 ·	95.04	73.89	75.32	72.02	74.45	66.17	
	$F \rightarrow 4$ )- $\beta$ -D-Glc $p$ -(1 $\rightarrow$	4.50	3.37	3.69	3.71	3.63	ND/ND	
	1 1)   2 3.0 (1	105.64	75.71	76.74	81.30	77.84	62.77	
	$\mathbf{G}$ →4)-β-D-Man $p$ -(1→	4.77	4.13	3.81	3.84	3.49	ND/ND	
	3 · 1) p 2 manp (1	103.27	72.79	74.28	79.88	77.84	62.77	
	H →4)-2-O-acetyl-β-D-Manp-(1→	4.95	5.52	4.02	3.86	3.64	ND/ND	
	11 - 1) 2 0 access p 2 manp (1	102.12	74.30	72.93	79.94	77.98	62.77	
	$I \rightarrow 4$ )-3-O-acetyl-β-D-Man $p$ -(1→	4.83	4.21	5.11	ND	ND	ND/ND	
	1 7 ) 5 5 decetyr p 2 Manp (1 7	102.66	71.47	76.38	ND	ND	62.77	
	$J \rightarrow 4$ )-6- <i>O</i> -acetyl- $\beta$ -D-Man <i>p</i> -(1 $\rightarrow$	ND	ND	ND	ND	ND	4.53/4.28	
	b 1) o o access p B manp (1	ND	ND	ND	ND	ND	65.89	
PKP-3	A β-D-Fruf-(2→	3.84/3.65	/	4.19	4.12	3.86	3.84/3.77	
	11   2 114) (2	62.84	106.72	79.41	77.55	83.94	65.05	
	$\mathbf{B} \rightarrow 6$ )- $\beta$ -D-Fruf-(2 $\rightarrow$	3.83/3.69	/	4.20	4.07	3.95	3.95/3.58	
	2 70) p 2 11d) (2 7	63.04	106.88	79.47	77.81	83.13	66.03	
	$C \rightarrow 1$ )- $\beta$ -D-Fruf- $(2 \rightarrow$	3.77/3.69	/	4.19	4.11	3.87	3.84/3.77	
	5 1) p D 11tg (2 /	63.35	106.57	79.64	77.26	83.98	65.17	
	$\mathbf{D} \rightarrow 1,6$ )- $\beta$ -D-Fruf-(2 $\rightarrow$	3.90/3.72	/	4.24	4.10	3.87	3.73/3.65	
	Σ 1,0) γ D 114 (2 /	63.67	106.10	79.90	77.40	84.08	65.43	
	$E \rightarrow 6$ )- $\alpha$ -D-Glcp-(1 $\rightarrow$	5.42	3.57	3.77	3.48	3.95	3.83/3.76	
	I →0)-u-D-Gi¢p-(1→	95.04	73.89	75.32	72.02	74.45	66.17	

<sup>\*</sup> ND, not determined.

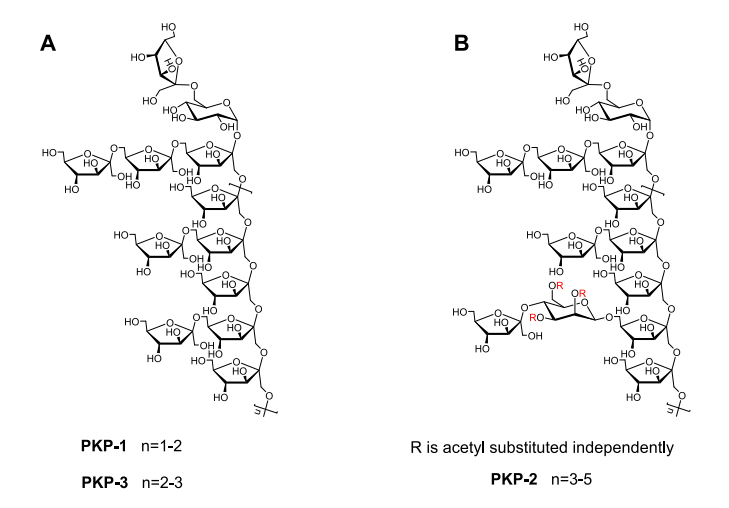


**Fig. 4.** Proposed chemical structures of three polysaccharides from *Polygonatum kingianum*. (A) The chemical structures of PKP-1 and PKP-3; (B) The chemical structures of PKP-2.

components such as acetyl groups and high molecular weight sugars [36].

The DSC plots showed the heat flow changes of the P. kingianum

polysaccharides at different temperatures. Three samples were observed to exhibit an exothermic peak around 80 °C indicating water evaporation at this temperature. Subsequently, a glass transition occurred at 200 °C, which was consistent with the analysis of the TG curve. There was an absorption peak around 400 °C, indicating that high-temperature carbonization has occurred at that temperature. The glass transition refers to the phase change of polymer materials from glassy to rubbery state [37], which is usually accompanied by the relaxation of molecular chains and the increase of free volume, and the heat absorption peaks of PKP-2 are more obvious than those of PKP-3, the relaxation of molecular chains is greater, and the increase of free volume is higher. The introduction of acetyl groups (e.g. PKP-2) will increase the hydrophobicity of the molecule. This can reduce the interaction between polymers and water, thereby potentially improving thermal stability and altering melting behavior [38]. Based on these two sets of data, it could be concluded that these polysaccharides have good thermal stability below 200 °C.

# 3.9. Rheological properties

All the three polysaccharides demonstrated high viscosity in the low shear rate region (Fig. 6A), with a significant decrease in viscosity correlating to an increase in shear rate. This phenomenon indicates that these polysaccharides exhibit shear thinning characteristics, which is a typical behavior of non-Newtonian fluids [39]. This means that under

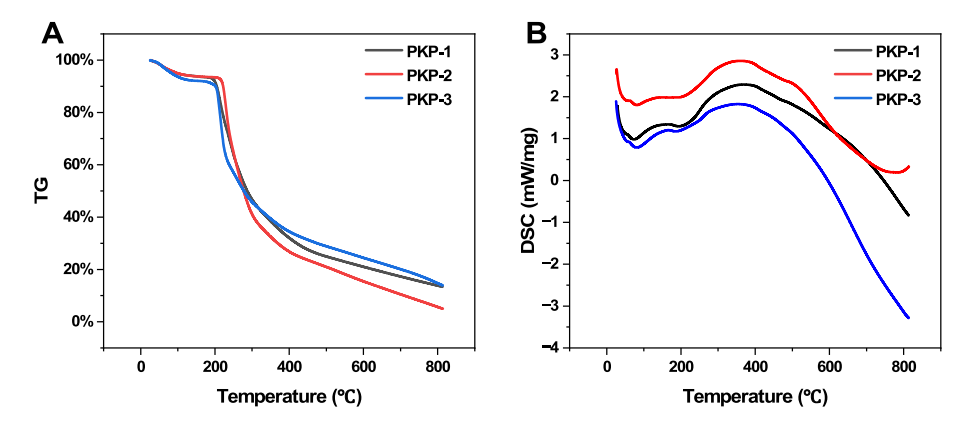
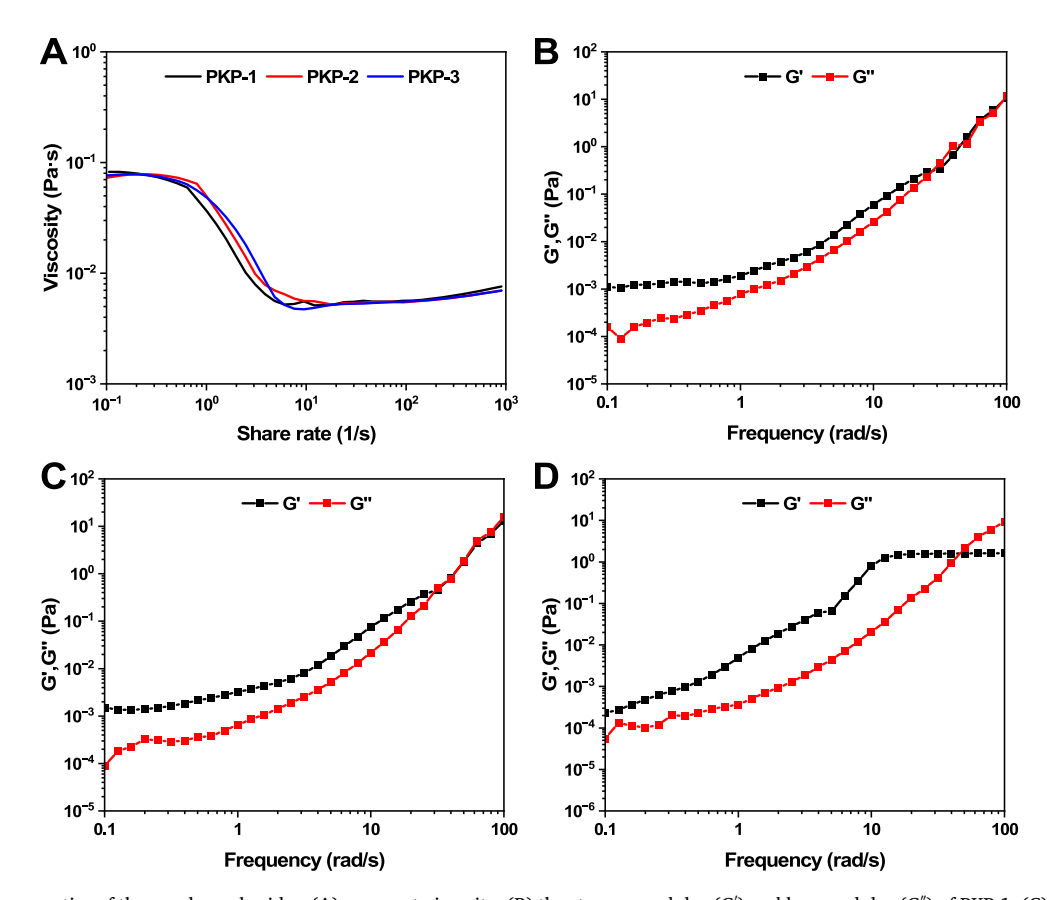


Fig. 5. Thermal characterization of three polysaccharides. (A) TG curves; (B) DSC curves.



**Fig. 6.** Rheological properties of three polysaccharides. (A) apparent viscosity; (B) the storage modulus (G') and loss modulus (G") of PKP-1; (C) the storage modulus (G') and loss modulus (G") of PKP-2; (D) the storage modulus (G') and loss modulus (G") of PKP-3.

conditions of high shear forces, such as during mixing or coating processes, these polysaccharides are likely to flow more easily. In the low shear rate region  $(10^{-1}-10^0~{\rm s}^{-1})$ , the viscosity of the three polysaccharides is similar, potentially suggesting similar molecular structures or compositions and fluidity when not subjected to substantial external forces. As the shear rate escalates, the three curves begin to separate. PKP-1 exhibits the fastest decrease in viscosity at moderate shear rates  $(10^0-10^1~{\rm s}^{-1})$ , while PKP-3 exhibits a slower decrease in viscosity at higher shear rates. The decrease in viscosity of PKP-2 across the entire shear rate range seems to be between PKP-1 and PKP-3. At extremely high shear rates  $(10^1-10^3~{\rm s}^{-1})$ , the viscosity of all polysaccharides tends to be lower and similar, indicating that under extreme conditions, these polysaccharides may exhibit similar fluidity.

Dynamic rheological measurements underscore that the storage (G')

and loss (G'') moduli of all polysaccharide solutions tested increased in a frequency-dependent manner, characteristic of macromolecular systems [40]. The observed intersections of G' and G'' across samples reflect a transition indicative of viscoelastic behavior-from a solid-like state at lower frequencies, where molecular chains can easily reorient, to a liquid-like state at higher frequencies, marked by the emergence of temporary networks [41]. Following the crossover point, molecular chains are impeded from unraveling during brief oscillations. This entanglement serves as a temporary cross-linking region at elevated frequencies, thereby manifesting the solid-like characteristics of viscoelastic materials, where the storage modulus (G') surpasses the loss modulus (G'') [36]. This transition is delayed in PKP-3 due to its lower polysaccharide concentration which prevents extensive cross-linking [42].

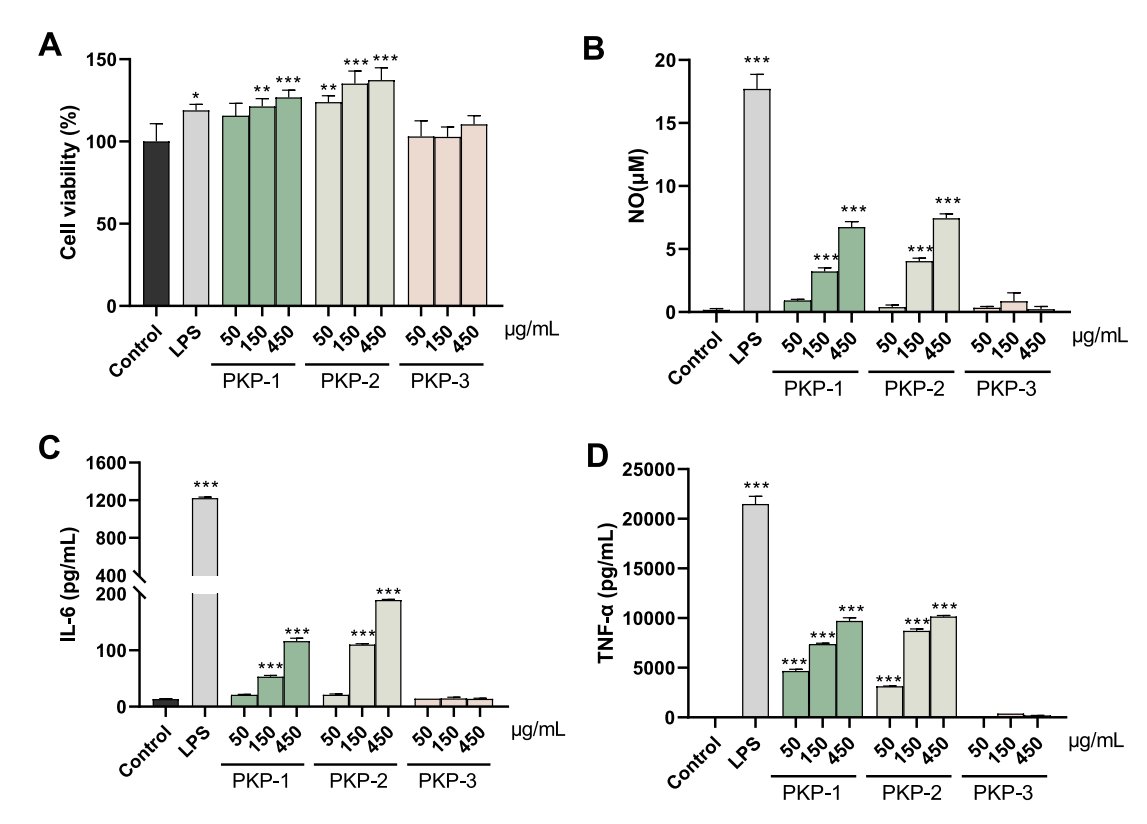


**Fig. 7.** Effects of the *Polygonatum kingianum* polysaccharides on activation of RAW264.7 macrophages. (A) Effects of these polysaccharides on the viability of RAW264.7 cells; (B) NO secretion levels; (C) IL-6 secretion levels; (D) TNF-α secretion levels. Data were presented as mean  $\pm$  SD (n = 3). \*P < 0.05, \*\*P < 0.01, \*\*\*P < 0.001 vs. the control group.

We had delved into the rheological properties and microstructure of three samples, which is crucial for understanding their potential applications in the food industry. By analyzing the rheological behavior of these samples in detail, we can reveal their key roles in syrup production and edible film manufacturing processes.

# 3.10. Immunomodulatory activity in vitro

#### 3.10.1. Effects of polysaccharides on RAW264.7 cells viability

The effects of *P. kingianum* polysaccharides on the viability of RAW264.7 cells were assessed using the CCK-8 method. RAW264.7 cells were incubated with different concentrations (50, 150, and 450  $\mu$ g/mL) of these polysaccharides for 24 h. As shown in Fig. 7A, the three polysaccharides had no significant inhibitory effect on the proliferation of RAW264.7 cells, while PKP-1 (450  $\mu$ g/mL) and PKP-2 (150  $\mu$ g/mL and 450  $\mu$ g/mL) could significantly promote the proliferation of RAW264.7 cells (P < 0.001).

# 3.10.2. Effects of polysaccharides on NO production

Macrophages, as the primary innate immune cells, can not only contribute to chronic inflammation but also to inhibit the development of cancer through the secretion of various factors and the modulation of other immune cells [43]. The production of nitric oxide (NO) by activated macrophages plays a crucial role in combating infectious and inflammatory diseases. The NO produced by macrophage activation is crucial in combating infectious and inflammatory diseases [44]. As shown in Fig. 7B, compared with the blank control group, LPS, PKP-1 (150  $\mu$ g/mL and 450  $\mu$ g/mL) and PKP-2 (150  $\mu$ g/mL and 450  $\mu$ g/mL) treatments were able to significantly promote the production of NO by RAW264.7 cells (P < 0.001) in a dose-dependent manner, while PKP-3 (50  $\mu$ g/mL, 150  $\mu$ g/mL and 450  $\mu$ g/mL) could not promote the NO secretion by RAW264.7 cells.

# 3.10.3. Effects of polysaccharides on cytokines secretion

Cytokines have powerful immunomodulatory effects that are critical to physiology and pathology in human [45]. To further elucidate the immunomodulatory activities of these P. kingianum polysaccharides, IL-6 and TNF-α contents in the supernatants of polysaccharides were measured by the ELISA method. Compared with the control group, the secretion of IL-6 and TNF- $\alpha$  was promoted in a dose-dependent manner after treatment with PKP-1 and PKP-2 (Fig. 7C-D) and was significantly promoted at 150  $\mu$ g/mL and 450  $\mu$ g/mL concentrations (P < 0.001). However, no significant differences were observed in IL-6 production under 50 µg/mL PKP-1 and PKP-2 treatments (Fig. 7C). In contrast, PKP-3 (50  $\mu g/mL$ , 150  $\mu g/mL$ , and 450  $\mu g/mL$ ) could not promote the secretion of IL-6 and TNF- $\alpha$ . These results suggested that PKP-1 and PKP-2 participate in the immune response by activating macrophages, showing potential immunomodulatory activities. Compared with chemical structures of these polysaccharides (Fig. 1 and Fig. 4), PKP-1 and PKP-2 have immunomodulatory effects on RAW 264.7 macrophages, including promoting cytokine and NO release, which may be attributed to their higher ratios of glucose to fructose and acetyl substitution in polysaccharides [6,51].

# 3.10.4. Effects of polysaccharides on the activation of NF-κB pathway

Nuclear factor- $\kappa B$  (NF- $\kappa B$ ) is a crucial class of transcription factors that regulates the survival, activation, and differentiation of innate immune cells and inflammatory T cells [46]. The NF- $\kappa B$  transcription factor family comprises five members: NF- $\kappa B$ 1 (p50), NF- $\kappa B$ 2 (p52), p65 (RELA), RelB, and c-Rel, which mediate NF- $\kappa B$  activity by forming homo- or hetero- dimers. The transcription of target genes is guided by these dimers, with p65/p50 being the most prevalent dimerized form [47,48]. In inactivated cells, I $\kappa B$  binds to NF- $\kappa B$ , sequestering it in the cytoplasm in an inactive form and thereby preventing NF- $\kappa B$  from entering the nucleus. Upon activation, I $\kappa B \alpha$  is phosphorylated by the I $\kappa B$  kinase (IKK) complex, subsequently ubiquitinated, and degraded via the

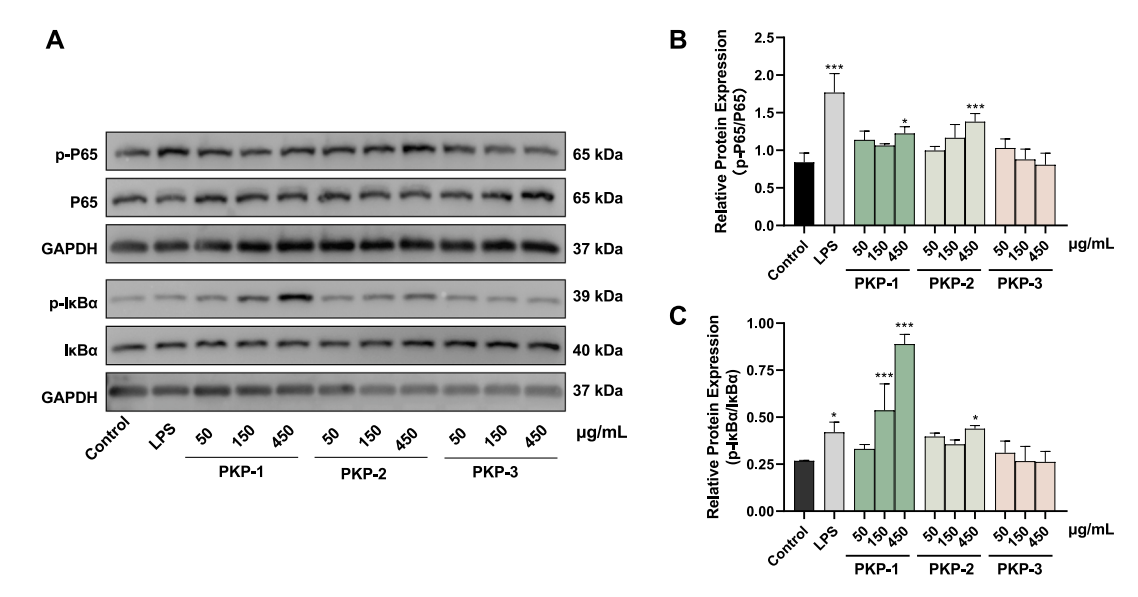


**Fig. 8.** Effects of *Polygonatum kingianum* polysaccharides on the expression of related proteins in the NF-κB signaling pathway. (A) Protein band plots of p-P65, P65, p-IκB-α and IκB-α. (B) The plot quantified the ratio of p-P65 to P65. (C) The plot quantified the ratio of p-IκB-α to IκB-α. Data were shown as mean  $\pm$  SD (n = 3). \*P < 0.05, \*\*P < 0.01, \*\*\*P < 0.01, \*\*\*P < 0.001 vs. the control group.

proteasome-dependent pathway, which releases NF- $\kappa$ B into the nucleus to activate the transcription of target genes [49,50]. To investigate whether these polysaccharides exert immunomodulatory effects by activating the NF- $\kappa$ B pathway, Western blot analysis was employed to assess the protein and phosphorylation levels of p65 and I $\kappa$ B $\alpha$  in the NF- $\kappa$ B pathway. As shown in Fig. 8A-C, the phosphorylation levels of p65 and I $\kappa$ B $\alpha$  were significantly elevated following treatment with LPS, PKP-1 (450 µg/mL), and PKP-2 (450 µg/mL) compared with the control group. In contrast, PKP-3 treatment did not produce a significant effect on the phosphorylation levels of p65 and I $\kappa$ B $\alpha$ . These findings indicate that PKP-1 and PKP-2 can activate the NF- $\kappa$ B signaling pathway by enhancing the phosphorylation of p65 and I $\kappa$ B $\alpha$  in RAW264.7 cells, which subsequently lead to increase secretion of NO, TNF- $\alpha$ , and IL-6, thereby exerting an immunoregulatory effect.

# 4. Conclusion

Three types of polysaccharides were isolated and purified from P. kingianum, including PKP-1, PKP-2, and PKP-3. By molecular weight measurement, monosaccharide composition analysis, methylation analysis and NMR analysis, it was found that PKP-1 has a higher glucose content, while PKP-2 contains acetyl groups. The three polysaccharides are all fructans belonging to Graminans series, and their structures lead to differences in surface morphology, thermal stability, rheological properties and immunomodulatory activity. SEM revealed significant differences in the surface morphology of the three polysaccharides. The results of thermal characterization showed that all three types of polysaccharides have high thermal stability. Rheological property analysis results showed that all three polysaccharides are typical shear-thinning fluids. Furthermore, the RAW264.7 macrophage assays indicated that PKP-1 and PKP-2 exhibited significant immunomodulatory activity, because they significantly enhanced the secretion of NO, TNF- $\alpha$ , and IL-6 by promoting the phosphorylation of P65 and  $I\kappa B-\alpha$ , and thereby activating the NF-κB signaling pathway. In contrast, PKP-3 did not possess this immunomodulatory activity. These findings suggested that PKP-1 and PKP-2 could be used as potential immunomodulatory dietary supplements.

# CRediT authorship contribution statement

Nanyu Chen: Writing - original draft, Visualization, Methodology,

Investigation, Formal analysis, Data curation, Conceptualization. Yunzhang Ding: Methodology, Investigation, Formal analysis, Data curation. Xuan Li: Methodology, Investigation, Formal analysis, Data curation. Jiang Li: Data curation, Formal analysis, Investigation, Methodology. Yongxian Cheng: Writing – review & editing, Supervision, Resources. Yong Tian: Funding acquisition, Conceptualization. Yuncai Tian: Funding acquisition, Conceptualization. Mingyi Wu: Writing – review & editing, Supervision, Methodology, Funding acquisition, Conceptualization.

# **Declaration of competing interest**

The authors declare that they have no known competing financial interests or personal relationships that could have appeared to influence the work reported in this paper.

# Data availability

Data will be made available on request.

# Acknowledgements

This work was supported by the National Youth Talent Support Program, Yunnan Fundamental Research Projects (Nos. 202201AS070073, 202301AV070008, and 202302AA310012), the Open Research Fund of Yunnan Characteristic Plant Extraction Laboratory (YKKF2023001), the National Natural Science Foundation of China (81930097), the Youth Innovation Promotion Association CAS (Y2021104), and the Ten-thousand Talents Program of Yunnan Province (YNWR-QNBJ-2018-271).

# Appendix A. Supplementary data

Supplementary data to this article can be found online at https://doi.org/10.1016/j.ijbiomac.2024.135406.

#### References

[1] S. Zhu, P. Liu, W. Wu, D. Li, E.-X. Shang, S. Guo, D. Qian, H. Yan, W. Wang, J. Duan, Multi-constituents variation in medicinal crops processing: investigation of nine cycles of steam-sun drying as the processing method for the rhizome of

- Polygonatum cyrtonema, J. Pharm. Biomed. Anal. 209 (2022) 114497, https://doi.org/10.1016/i.jpba.2021.114497.
- [2] H.K. Xue, W.L. Wang, J.Y. Bian, Y.C. Gao, Z.T. Hao, J.Q. Tan, Recent advances in medicinal and edible homologous polysaccharides: extraction, purification, structure, modification, and biological activities, Int. J. Biol. Macromol. 222 (2022) 1110–1126, https://doi.org/10.1016/j.ijbiomac.2022.09.227.
- [3] Y. Hu, Y. Tang, Z. Zhang, X. Guo, Z. Wu, Z. Li, H. Yu, W. Li, Recent advances in polysaccharides from the genus *Polygonatum*: isolation, structures, bioactivities, and application, Food Hydrocoll. 140 (2023) 108634, https://doi.org/10.1016/j. foodhyd.2023.108634.
- [4] S. Zheng, Protective effect of *Polygonatum sibiricum* polysaccharide on D-galactose-induced aging rat model, Sci. Rep. 10 (1) (2020) 2246, https://doi.org/10.1038/s41598-020-59055-7
- [5] S. Wang, G. Li, X. Zhang, Y. Wang, Y. Qiang, B. Wang, J. Zou, J. Niu, Z. Wang, Structural characterization and antioxidant activity of *Polygonatum sibiricum* polysaccharides, Carbohydr. Polym. 291 (2022) 119524, https://doi.org/10.1016/ j.carbpol.2022.119524.
- [6] P. Zhao, H. Zhou, C. Zhao, X. Li, Y. Wang, Y. Wang, L. Huang, W. Gao, Purification, characterization and immunomodulatory activity of fructans from *Polygonatum odoratum* and *P. cyrtonema*, Carbohydr. Polym. 214 (2019) 44–52, https://doi.org/10.1016/j.carbpol.2019.03.014.
- [7] Y. Luo, Q. Fang, Y. Lai, H. Lei, D. Zhang, H. Niu, R. Wang, C. Song, Polysaccharides from the leaves of *Polygonatum sibiricum* Red. regulate the gut microbiota and affect the production of short-chain fatty acids in mice, AMB Express 12 (1) (2022) 35, https://doi.org/10.1186/s13568-022-01376-z.
- [8] J. Zhang, H. Chen, L. Luo, Z. Zhou, Y. Wang, T. Gao, L. Yang, T. Peng, M. Wu, Structures of fructan and galactan from *Polygonatum cyrtonema* and their utilization by probiotic bacteria, Carbohydr. Polym. 267 (2021) 118219, https://doi.org/ 10.1016/j.carbpol.2021.118219.
- [9] M. Girard, C. Schaffer-Lequart, Gelation of skim milk containing anionic exopolysaccharides and recovery of texture after shearing, Food Hydrocoll. 21 (7) (2007) 1031–1040, https://doi.org/10.1016/j.foodhyd.2006.07.012.
- [10] D.K. Shen, S. Gu, A.V. Bridgwater, The thermal performance of the polysaccharides extracted from hardwood: cellulose and hemicellulose, Carbohydr. Polym. 82 (1) (2010) 39–45, https://doi.org/10.1016/j.carbpol.2010.04.018.
- [11] Y. Wu, Z. Zhou, L. Luo, M. Tao, X. Chang, L. Yang, X. Huang, L. Hu, M. Wu, A non-anticoagulant heparin-like snail glycosaminoglycan promotes healing of diabetic wound, Carbohydr. Polym. 247 (2020) 116682, https://doi.org/10.1016/j.carbol 2020.116682
- [12] J. Liu, F.N. Shang, Z.M. Yang, M.Y. Wu, J.H. Zhao, Structural analysis of a homogeneous polysaccharide from *Achatina fulica*, Int. J. Biol. Macromol. 98 (2017) 786–792, https://doi.org/10.1016/j.ijbiomac.2017.01.149.
- [13] T. Zhang, J. Ye, C. Xue, Y. Wang, W. Liao, L. Mao, M. Yuan, S. Lian, Structural characteristics and bioactive properties of a novel polysaccharide from *Flammulina velutipes*, Carbohydr. Polym. 197 (2018) 147–156, https://doi.org/10.1016/j.carbpol.2018.05.069.
- [14] J. Zhang, M. Chen, C. Wen, J. Zhou, J. Gu, Y. Duan, H. Zhang, X. Ren, H. Ma, Structural characterization and immunostimulatory activity of a novel polysaccharide isolated with subcritical water from Sagittaria sagittifolia L, Int. J. Biol. Macromol. 133 (2019) 11–20, https://doi.org/10.1016/j. iibiomac.2019.04.077.
- [15] Y. Cheng, X. Xiao, X. Li, D. Song, Z. Lu, F. Wang, Y. Wang, Characterization, antioxidant property and cytoprotection of exopolysaccharide-capped elemental selenium particles synthesized by *Bacillus paralicheniformis* SR14, Carbohydr. Polym. 178 (2017) 18–26, https://doi.org/10.1016/j.carbpol.2017.08.124.
- [16] N. Li, C. Shi, S. Shi, H. Wang, J. Yan, S. Wang, An inulin-type fructan isolated from Artemisia japonica and its anti-arthritic effects, J. Funct. Foods 29 (2017) 29–36, https://doi.org/10.1016/j.iff.2016.11.033.
- [17] J. Xu, D. Chen, C. Liu, X.Z. Wu, C.X. Dong, J. Zhou, Structural characterization and anti-tumor effects of an inulin-type fructan from *Atractylodes chinensis*, Int. J. Biol. Macromol. 82 (2016) 765–771, https://doi.org/10.1016/j.ijbiomac.2015.10.082.
- [18] P. Peng, F. Peng, J. Bian, F. Xu, R. Sun, Studies on the starch and hemicelluloses fractionated by graded ethanol precipitation from bamboo *Phyllostachys* bambusoides f. shouzhu Yi, J. Agric. Food Chem. 59 (6) (2011) 2680–2688, https:// doi.org/10.1021/if1045766.
- [19] W. Wei, L. Feng, W.R. Bao, D.L. Ma, C.H. Leung, S.P. Nie, Q.B. Han, Structure characterization and immunomodulating effects of polysaccharides isolated from *Dendrobium officinale*, J. Agric. Food Chem. 64 (4) (2016) 881–889, https://doi. org/10.1021/acs.jafc.5b05180.
- [20] F.A. Pettolino, C. Walsh, G.B. Fincher, A. Bacic, Determining the polysaccharide composition of plant cell walls, Nat. Protoc. 7 (9) (2012) 1590–1607, https://doi. org/10.1038/nprot.2012.081.
- [21] I. Speciale, A. Notaro, P. Garcia-Vello, F. Di Lorenzo, S. Armiento, A. Molinaro, R. Marchetti, A. Silipo, C. De Castro, Liquid-state NMR spectroscopy for complex carbohydrate structural analysis: a hitchhiker's guide, Carbohydr. Polym. 277 (2022) 118885, https://doi.org/10.1016/j.carbpol.2021.118885.
- [22] X.M. Chen, G.Y. Tian, Structural elucidation and antitumor activity of a fructan from Cyathula officinalis Kuan, Carbohydr. Res. 338 (11) (2003) 1235–1241, https://doi.org/10.1016/s0008-6215(03)00073-9.
- [23] M.G. Lopez, N.A. Mancilla-Margalli, G. Mendoza-Diaz, Molecular structures of fructans from Agave tequilana Weber var. azul, J. Agric. Food Chem. 51 (27) (2003) 7835–7840, https://doi.org/10.1021/jf030383v.
- [24] Y. Liu, X. Duan, M. Zhang, C. Li, Z. Zhang, B. Hu, A. Liu, Q. Li, H. Chen, Z. Tang, W. Wu, D. Chen, Extraction, structure characterization, carboxymethylation and antioxidant activity of acidic polysaccharides from *Craterellus cornucopioides*, Ind. Crop. Prod. 159 (2021) 113079, https://doi.org/10.1016/j.indcrop.2020.113079.

- [25] C. Teng, P. Qin, Z. Shi, W. Zhang, X. Yang, Y. Yao, G. Ren, Structural characterization and antioxidant activity of alkali-extracted polysaccharides from quinoa, Food Hydrocoll. 113 (2021) 106392, https://doi.org/10.1016/j. foodbyd/2020.106392
- [26] C. Wang, D. Hua, C. Yan, Structural characterization and antioxidant activities of a novel fructan from Achyranthes bidentata Blume, a famous medicinal plant in China, Ind. Crop. Prod. 70 (2015) 427–434, https://doi.org/10.1016/j. indexep. 2015.03.051
- [27] W. Liu, L. Zhang, X. Wei, Y. Xu, Q. Fang, S. Qi, J. Chen, C. Wang, S. Wang, L. Qin, P. Liu, J. Wu, Structural characterization of an inulin neoseries-type fructan from Ophiopogonis Radix and the therapeutic effect on liver fibrosis in vivo, Carbohydr. Polym. 327 (2024) 121659, https://doi.org/10.1016/j.carbpol.2023.121659.
- [28] L.H. Campestrini, J.L. Silveira, M.E. Duarte, H.S. Koop, M.D. Noseda, NMR and rheological study of *Aloe barbadensis* partially acetylated glucomannan, Carbohydr. Polym. 94 (1) (2013) 511–519, https://doi.org/10.1016/j.carbpol.2013.01.020.
- [29] Y. Deng, L.-X. Chen, B.-X. Han, D.-T. Wu, K.-L. Cheong, N.-F. Chen, J. Zhao, S.-P. Li, Qualitative and quantitative analysis of specific polysaccharides in *Dendrobium huoshanense* by using saccharide mapping and chromatographic methods, J. Pharm. Biomed. Anal. 129 (2016) 163–171, https://doi.org/10.1016/j. ipha. 2016.06.051
- [30] M.-T. Kuang, J.-Y. Li, X.-B. Yang, L. Yang, J.-Y. Xu, S. Yan, Y.-F. Lv, F.-C. Ren, J.-M. Hu, J. Zhou, Structural characterization and hypoglycemic effect via stimulating glucagon-like peptide-1 secretion of two polysaccharides from *Dendrobium officinale*, Carbohydr. Polym. 241 (2020) 116326, https://doi.org/10.1016/j.carbpol.2020.116326.
- [31] Q. Gu, Y. Liu, L. Zhen, T. Zhao, L. Luo, J. Zhang, T. Deng, M. Wu, G. Cheng, J. Hu, The structures of two glucomannans from *Bletilla formosana* and their protective effect on inflammation via inhibiting NF-κB pathway, Carbohydr. Polym. 292 (2022) 119694, https://doi.org/10.1016/j.carbpol.2022.119694.
- [32] F. Di Bartolomeo, W. Van den Ende, Fructose and fructans: opposite effects on health? Plant Foods Hum. Nutr. 70 (3) (2015) 227–237, https://doi.org/10.1007/ s11130-015-0485-6.
- [33] Y. Tang, X. He, G. Liu, Z. Wei, J. Sheng, J. Sun, C. Li, M. Xin, L. Li, P. Yi, Effects of different extraction methods on the structural, antioxidant and hypoglycemic properties of red pitaya stem polysaccharide, Food Chem. 405 (2023) 134804, https://doi.org/10.1016/j.foodchem.2022.134804.
- [34] L.S. Ma, H.X. Chen, Y. Zhang, N. Zhang, L.L. Fu, Chemical modification and antioxidant activities of polysaccharide from mushroom, Carbohydr. Polym. 89 (2) (2012) 371–378, https://doi.org/10.1016/j.carbpol.2012.03.016.
- [35] H. Postulkova, I. Chamradova, D. Pavlinak, O. Humpa, J. Jancar, L. Vojtova, Study of effects and conditions on the solubility of natural polysaccharide gum karaya, Food Hydrocoll. 67 (2017) 148–156, https://doi.org/10.1016/j. foodhyd.2017.01.011.
- [36] D.M. de Carvalho, J. Berglund, C. Marchanda, M.E. Lindström, F. Vilaplana, O. Sevastyanova, Improving the thermal stability of different types of xylan by acetylation, Carbohydr. Polym. 220 (2019) 132–140, https://doi.org/10.1016/j. carbpol.2019.05.063.
- [37] B. Borde, H. Bizot, G. Vigier, A. Buléon, Calorimetric analysis of the structural relaxation in partially hydrated amorphous polysaccharides. II. Phenomenological study of physical ageing, Carbohydr. Polym. 48 (2) (2002) 111–123, https://doi. org/10.1016/S0144-8617(01)00218-1.
- [38] X.M. Zhou, X.X. Lin, K.L. White, S. Lin, H. Wu, S.L. Cao, L.L. Huang, L.H. Chen, Effect of the degree of substitution on the hydrophobicity of acetylated cellulose for production of liquid marbles, Cellulose 23 (1) (2016) 811–821, https://doi.org/ 10.1007/s10570-015-0856-2
- [39] M. Hamdi, R. Nasri, S. Hajji, M. Nigen, S.M. Li, M. Nasri, Acetylation degree, a key parameter modulating chitosan rheological, thermal and film-forming properties, Food Hydrocoll. 87 (2019) 48–60, https://doi.org/10.1016/j. foodhyd.2018.07.027.
- [40] L. Lin, M. Shen, S. Liu, W. Tang, Z. Wang, M. Xie, J. Xie, An acidic heteropolysaccharide from *Mesona chinensis*: rheological properties, gelling behavior and texture characteristics, Int. J. Biol. Macromol. 107 (Pt B) (2018) 1591–1598, https://doi.org/10.1016/j.ijbiomac.2017.10.029.
- [41] M. Yoshimura, T. Takaya, K. Nishinari, Rheological studies on mixtures of corn starch and konjac-glucomannan, Carbohydr. Polym. 35 (1–2) (1998) 71–79, https://doi.org/10.1016/S0144-8617 (97)00232-4.
- [42] M.G. Sosa-Herrera, L.P. Martínez-Padilla, V.A. Delgado-Reyes, M.D.D. Ortega, I.P. C. Martínez, Effect of agave fructans on xanthan rheology: impact on sodium caseinate emulsion properties, J. Food Sci. 87 (7) (2022) 2858–2868, https://doi.org/10.1016/j.carbpol.2021.118885.
- [43] Z. Duan, Y. Luo, Targeting macrophages in cancer immunotherapy, Signal Transduct. Target. Ther. 6 (1) (2021) 127, https://doi.org/10.1038/s41392-021-00506-6.
- [44] S. Tang, M. Jiang, C. Huang, C. Lai, Y. Fan, Q. Yong, Characterization of arabinogalactans from *Larix principis-rupprechtii* and their effects on NO production by macrophages, Carbohydr. Polym. 200 (2018) 408–415, https://doi.org/ 10.1016/j.carbpol.2018.08.027.
- [45] X. Zheng, Y. Wu, J. Bi, Y. Huang, Y. Cheng, Y. Li, Y. Wu, G. Cao, Z. Tian, The use of supercytokines, immunocytokines, engager cytokines, and other synthetic cytokines in immunotherapy, Cell. Mol. Immunol. 19 (2) (2022) 192–209, https:// doi.org/10.1038/s41423-021-00786-6.
- [46] D. Capece, D. Verzella, I. Flati, P. Arboretto, J. Cornice, G. Franzoso, NF-κB: blending metabolism, immunity, and inflammation, Trends Immunol. 43 (9) (2022) 757–775, https://doi.org/10.1016/j.it.2022.07.004.
- [47] T. Zhang, C. Ma, Z. Zhang, H. Zhang, H. Hu, NF- $\kappa$ B signaling in inflammation and cancer, MedComm 2 (4) (2021) 618–653, https://doi.org/10.1002/mco2.104.

- [48] T. Liu, L. Zhang, D. Joo, S.-C. Sun, NF-κB signaling in inflammation, Signal Transduct. Target. Ther. 2 (1) (2017) 17023, https://doi.org/10.1038/sigtrans 2017 23
- [49] B. Hoesel, J.A. Schmid, The complexity of NF-кВ signaling in inflammation and cancer, Mol. Cancer 12 (1) (2013) 86, https://doi.org/10.1186/1476-4598-12-86.
- [50] Q. Li, I.M. Verma, NF- $\kappa$ B regulation in the immune system, Nat. Rev. Immunol. 2 (10) (2002) 725–734, https://doi.org/10.1038/nri910.
- [51] L. Sun, L. Wang, Y. Zhou, Immunomodulation and antitumor activities of different-molecular-weight polysaccharides from *Porphyridium cruentum*, Carbohydr. Polym. 87 (2) (2012) 1206–1210, https://doi.org/10.1016/j.carbpol.2011.08.097.